

**Coherent lattice dynamics in opaque crystals: Testing the adequacy of two-tensor model**O. V. Misochko<sup>1,2,\*</sup> and M. V. Lebedev<sup>1,2</sup><sup>1</sup>*Institute of Solid State Physics, Russian Academy of Sciences, Chernogolovka, Moscow Region 142432, Russia*<sup>2</sup>*Institute of Nanotechnologies of Microelectronics, Russian Academy of Sciences, Moscow 119334, Russia*

(Received 24 June 2016; revised manuscript received 15 September 2016; published 17 November 2016)

We report the ultrafast pump-probe study of Bi<sub>2</sub>Te<sub>3</sub>, Sb, Bi, and Te aimed to check the two-tensor model predictions for the creation of lattice coherence. The dependence of coherent ultrafast response on phonon frequency was measured for topological insulator Bi<sub>2</sub>Te<sub>3</sub>, the spectrum of which possesses two fully symmetric phonons. The effect of the pump pulse duration and power on the magnitude of coherent amplitude was evaluated in the model opaque crystals, such as two semimetals, bismuth and antimony, and semiconducting tellurium. In our analysis of the pump-probe data, we separated the transient total reflectivity into the sum of two contributions: one due to the photogenerated carriers and the second due to the coherent phonons. All fully symmetric phonons exhibit a cosinelike dependence and grow linearly with increasing average pump power provided the pulse duration remains unchanged. Varying the pump pulse duration, we observed a monotonic decrease of coherent amplitude for longer pulses, whereas the electronic contribution was almost unchanged. This lack of the correlation between the carriers and the coherent amplitude was further supported by coherent control experiments on Te. Based on the comparison of theoretical predictions with experimental observations, we conjecture that the lattice coherence creation in opaque crystals can be linked to a Raman-like process.

DOI: [10.1103/PhysRevB.94.184307](https://doi.org/10.1103/PhysRevB.94.184307)**I. INTRODUCTION**

A femtosecond laser pulse is shorter in duration than the time required for elementary atomic motion in condensed matter. This feature leads to a variety of the novel effects which occur unavoidably when such a pulse propagates through or reflects off almost any material. For example, it has become possible to monitor the atomic motion by creating coherent phonons and conducting observations on time scales that are shorter than the phonon period. Coherence is a unique property of quantum mechanics that allows electrons to move without dissipation and elementary excitations to be in two states at once. The coherence of crystal lattice, the inevitable result of ultrafast excitation, can be created either via a Raman mechanism that requires a broad enough pulse spectrum or, alternatively, via fast radiationless transitions of an optically pumped electronic state, which need a steep temporal profile for the pump pulse.

Ultrashort laser pulses have been extensively used in the past decades to study and manipulate the coherent lattice dynamics in a variety of materials [1–4]. The high degree of temporal and spatial coherence created in the lattice by an ultrashort pulse is convincingly confirmed by optical control experiments in which the second pump pulse either enhances or annihilates one of the superposition components [4]. However, virtually all ultrafast experiments so far have been limited to a particular pulse duration which is shorter than inverse phonon frequency while the effect of pulse width on coherent phonon generation remains essentially unexplored. The visible and near-infrared light does not couple with crystal lattice in a direct way due to a huge energy mismatch between photons and phonons. Therefore, lattice coherence in an ultrafast experiment is always created via an electron-phonon coupling, and to identify the coherent phonon generation mechanism one

has to establish the correct form of the coupling. There are two excitation schemes most commonly used for coherent phonon generation: impulsive stimulated Raman scattering (ISRS) which can occur with off-resonant or resonant excitation wavelengths [1,4] and impulsive absorption which takes place on resonance and has been labeled displacive excitation of coherent phonons (DECP) [5]. Light coherence is transferred to the lattice for the former but not for the latter, in which the lattice coherence is an emerging property. While it is well established that ISRS serves as the driving force for the coherent phonons in the spectral region where materials are transparent, there is still a dispute about the underlying mechanisms in the opaque regime. One point of view is that DECP is a unique excitation mechanism unrelated to Raman scattering [5,6]. Another point of view is that DECP can be reduced to a resonant Raman mechanism [2]. Indeed, it was suggested some time ago ISRS should be controlled not by single but by two different tensors [2,7,8]. One is the standard Raman tensor, the same one that is responsible for spontaneous Raman scattering intensity, and a second tensor associated with the driving force of coherent phonon amplitude [7,8]. The real parts of these two tensors are the same and, as a result, there is a single tensor for transparent materials in which the light-induced driving force is proportional to standard Raman polarizability and behaves impulsively for pulses shorter than the phonon period. Alternatively, in absorbing regions, the second tensor is the one that takes part in the coherent phonon generation. As the imaginary parts of both tensors in the absorbing region differ considerably, by using the proper tensor, it is possible to reproduce the impulsive behavior in the transparent and the displacive behavior in the opaque regime [8].

The paper is aimed at clarifying the validity of the two-tensor model through the comparison of its predictions with those of DECP and experimental data. Its goal is to compare two coherent phonons in Bi<sub>2</sub>Te<sub>3</sub> crystal, which have the same full symmetry but are different in frequency, and, additionally, to study fully symmetric phonons in two model semimetals

\*misochko@issp.ac.ru

and a semiconductor as a function of the pump pulse duration and power. Such study should clarify the applicability of the two-tensor model for explaining the coherent lattice dynamics in the opaque regime. We attempt to investigate the link between the electronic excitations and the fully symmetric coherent phonons as well as their dependence on pulse duration in the materials where DECP is identified as the generating mechanism. Such comparison can help identify whether the DECP and two-tensor models are identical. The paper is outlined as follows. In Sec. II, we briefly consider a number of testable predictions of DECP and two-tensor model, while in Sec. III we address the technical aspects regarding the samples and the setups for pump-probe technique and Raman spectroscopy. In Sec. IV, we show and discuss our experimental results. Finally, Sec. V contains the conclusions of the work.

## II. BASIC CONCEPTS

Before proceeding into a detailed discussion of our experiments, it is perhaps useful to make use of a general description that provides a physical explanation for the theories required to understand the processes of interest. First, consider the basics of coherent phonon excitation. The different generation mechanisms all have in common that an ultrashort laser pulse either almost instantaneously creates a new carrier distribution that the lattice atoms have to adjust to (displacive mechanism, kinematic excitation), or that it causes a short and intensive force on the atoms (impulsive mechanism, dynamic excitation) [1,2,4]. In both cases, the electronic system changes on a very short time scale, and after that does not contribute to the generation process anymore. Both ISRS and DECP mechanisms are based on the same general equation of motion, describing the time dependence of the phonon normal coordinate  $Q$  by the means of a kicked harmonic oscillator with unit mass

$$\frac{d^2Q}{dt^2} + 2\gamma \frac{dQ}{dt} + \Omega^2 Q = F(t), \quad (1)$$

where  $\Omega$  is the phonon frequency,  $\gamma$  is the phonon damping constant, and  $F(t)$  denotes the driving force. Equation (1) can be integrated formally, using either Green's functions or Laplace transforms with the initial condition that both  $Q$  and  $\partial Q/\partial t$  are zero before the force is applied, to give

$$Q(t) = \int_0^t \frac{F(\tau) e^{-\gamma(t-\tau)} \sin[\sqrt{\Omega^2 - \gamma^2}(t-\tau)]}{\sqrt{\Omega^2 - \gamma^2}} d\tau. \quad (2)$$

As the phenomenological oscillator model captures the essential physics, let us consider two limiting kinds of driving force. The first is a displacive force  $F(t) = D\vartheta(t)$  and the second, an impulsive one  $F(t) = I\delta(t)$ , where  $\vartheta(t)$  and  $\delta(t)$  are the Heaviside step and the Dirac delta function both centered on  $t = 0$  while  $D$  and  $I$  scale the force. For the displacive excitation, after integrating Eq. (2) we have

$$Q(t) = \frac{D\vartheta(t)}{\Omega^2} \left\{ 1 - e^{-\gamma t} \left[ \cos(t\sqrt{\Omega^2 - \gamma^2}) + \frac{\gamma}{\sqrt{\Omega^2 - \gamma^2}} \sin(t\sqrt{\Omega^2 - \gamma^2}) \right] \right\}. \quad (3)$$

The solution (3) shows the response consists of two contributions: a constant and an oscillatory part. In the following, we refer to the oscillatory part as the coherent contribution and the nonoscillatory part as the incoherent contribution. The incoherent, zero-frequency part can be attributed to the change of equilibrium position, while the oscillatory part is associated with a damped coherent oscillation. As far as coherent phonons are concerned, the DECP theory assumes that the pump pulse with duration shorter than inverse phonon frequency gets absorbed by the opaque material and alters the band and temperature distribution of the electrons [5]. The photoexcited electrons in the number proportional to the absorbed energy introduce a displacement of the equilibrium position of the atoms. This displacement preserves the unit cell symmetry and sets the atoms oscillating around the new equilibrium position. Other Raman modes lower the symmetry of the unit cell and thus are not the favorable displacement upon electronic excitation. It is the equilibrium coordinate that gets shifted by the electronic excitations and the “pushing force” that starts the oscillations and is governed by the excitation and relaxation of charge carriers. Since no momentum is imparting to atoms by the driving force action, the excitation has a kinematic character. Perhaps, it is appropriate to mention here that even though the generation of lattice coherence in the DECP model is not directly related to a Raman process, the detection of coherent phonons always requires a strong Raman scattering at phonon frequency [5]. Assuming a Gaussian pulse shape, the driving force—being a convolution of the pump pulse with the Heaviside function—for the displacive excitation takes the form

$$F_D(t) \propto \text{Im}(\varepsilon) E_{\text{int}} \text{erfc}\left(-\frac{t}{\tau_p}\right), \quad (4)$$

where  $\text{Im}(\varepsilon)$  is the imaginary part of the dielectric function  $\varepsilon$ ,  $E_{\text{int}}$  is the integrated pulse energy, and

$$\text{erfc}\left(-\frac{t}{\tau_p}\right) = \frac{2}{\sqrt{\pi}} \int_{t/\tau_p}^{\infty} \exp(-x^2) dx \quad (5)$$

is the complementary error function representing the rising edge of the driving force. The lower bound of this exponential integral function is determined by the laser pulse duration  $\tau_p$  that must be smaller than inverse phonon frequency,  $\Omega\tau_p < 1$ .

For the impulsive force, which provides a dynamical character of the excitation, after integrating Eq. (2), we get

$$Q(t) = \frac{I}{\sqrt{\Omega^2 - \gamma^2}} e^{-\gamma t} \sin(t\sqrt{\Omega^2 - \gamma^2})\theta(t). \quad (6)$$

From Eq. (6) follows that the impulsive force starts oscillations about the unchanged equilibrium position. For a Raman mechanism, in which the driving force occurs through mixing among frequency components of the electromagnetic field contained within the bandwidth of a transform-limited Gaussian pump pulse [1], the force has the form

$$F_R(\tau) \propto \chi I_0 e^{-\frac{\Omega^2 \tau^2}{4}}, \quad (7)$$

where  $\chi$  is the Raman tensor,  $I_0$  is the pulse integrated intensity, and the exponential term reflects the requirement that the laser pulse width  $\tau_p$  for efficient coherent excitation should be short compared to a single phonon period. The last requirement

can also be understood from the perspective of the frequency domain: the bandwidth of an ultrashort laser pulse needs to be wide enough to satisfy energy conservation with respect to the generated phonon frequency. In principle, Raman scattering can be thought of as a wave mixing process where one of the participating waves is given by the phonon. The nonlinear polarization, which depends quadratically on the electric field of laser light, has frequency components at the sum and difference between the phonon mode and the laser light frequency (the so-called anti-Stokes and Stokes frequencies, respectively). Note that any induced lattice motion is sensitive only to the laser intensity and not to the electric field directly. The response can be easily calculated using a Green's function analysis for any driving pulse shape [9]. It confirms that the coherence strength is proportional to the power spectral density of the pulse intensity envelope at the phonon frequency.

In contrast to DECP, in the off-resonant Raman case, the atoms (not the potential on which they reside) receive a “kick” imparting a certain momentum. Assuming that the pulse appears at the moment  $t = 0$  and is nonzero within the time interval of the pulse duration  $\tau_p$ , one finds that after the interaction, that is, for  $t > \tau_p$ , the coordinate exhibits freely damping oscillations. The displacement of the atom during the laser pulse action is much smaller, by a factor  $\tau_p \gamma \ll 1$ , than the amplitude of subsequent free oscillations because the atom acquires some initial velocity, but its coordinate has no time to change [10]. The difference between the impulsive and displacive force is easily seen from the illustrative example of a driven mechanical oscillator (a mass  $m$  on the spring of stiffness  $k$ ). Here one can relate the force magnitude  $F$  to the displacement  $|A|$ :

$$G(\omega) = \frac{|A|}{F} = \frac{1}{\sqrt{(-m\omega^2 + k)^2 + (\gamma\omega)^2}}. \quad (8)$$

At zero excitation frequency, we have  $G(0) = 1/k$ . This means that applying a constant force, we expect to stretch the spring by a constant amount and, since nothing is changing in time, both mass and drag are irrelevant. The proportionality between force and displacement is the stiffness, which appears here as  $1/k$  because we ask how much displacement one gets for a fixed force, rather than the other way around. At very high frequencies, the  $m\omega^2$  term is bigger than all the others, and so we find  $G(\omega \rightarrow \infty) = 1/m\omega^2$ , which means that pushing the oscillator at very high frequencies one hardly feels the stiffness or damping at all. What is felt instead is the inertia provided by the mass, and the applied force goes into accelerating this mass. This means that the high frequencies are responsible for a dynamic excitation, while the low frequencies result in a kinematic regime. Using a bit more sophisticated model, in the framework of an electronic circuit model [11], the distinct difference between DECP (kinematic) and Raman-like (dynamic) excitations was described as follows: the excitation takes place due to a low-frequency component of the pulse envelope for the former, whereas the system excitation is a kind of homo/heterodyning process due to mixing the carrier frequencies for the latter.

The Raman tensor  $\chi$ , which controls the force magnitude, can be expressed as the partial derivative of the dielectric tensor  $\varepsilon$  with respect to the phonon normal coordinate  $\chi(\omega, \omega \pm \Omega) \propto$

$\partial\varepsilon/\partial Q$  where  $\omega$  denotes the light angular frequency. While in the transparent regions, the tensor has its standard form

$$\chi_{kl}^R(\omega, \omega \pm \Omega) \propto \left\{ \frac{\partial \text{Re}[\varepsilon(\omega)]}{\partial \omega} + i \frac{\partial \text{Im}[\varepsilon(\omega)]}{\partial \omega} \right\}, \quad (9)$$

in the absorbing media, where  $\text{Im}(\varepsilon) \gg \text{Re}(\varepsilon)$ , the tensor responsible for coherent phonon generation is changed to

$$\chi_{kl}^Q(\omega, \omega \pm \Omega) \propto \left\{ \frac{\partial \text{Re}[\varepsilon(\omega)]}{\partial \omega} \mp i \frac{2\text{Im}[\varepsilon(\omega)]}{\Omega} \right\} \quad (10)$$

due to a different pole structure for the generation and scattering process [7,8]. Another important feature of the two-tensor model lies in the specific temporal profile of driving force. For transparent materials,  $\partial \text{Re}[\varepsilon(\omega)]/\partial \omega$  dominates, and the driving force follows the temporal shape of the pump pulse, a characteristic of impulsive excitation. For opaque materials,  $2\text{Im}[\varepsilon(\omega)]/\Omega$  controls the generation, therefore, the driving force has an error-function temporal profile, indicative of displacive excitation. Thus, a transiently stimulated Raman scattering mechanism can be extended from transparent to opaque materials since both the virtual and real electronic excitations are incorporated into the complex Raman tensor in the two-tensor model [7,8]. Further improvement of this unified model was made after the inclusion of lifetime effects for the driving force [12]. It was shown that when the force decay rate  $\Gamma$  is small, the force looks like a step function with its rising edge broadened by the pulse duration and lasting as long as  $1/\Gamma \gg 1/\Omega$ . On the other hand, when the decay rate increases, the force gradually transforms to a bell-like shape with its amplitude inversely related to the decay rate magnitude [13].

Let us summarize the relations between the magnitude of coherent amplitude  $Q_0$ , which we define as the amplitude of free damped oscillations after the interaction is over, and the experimentally controlled parameters for the different generation scenarios. From Eqs. (2), (4), and (7) it follows that the coherent amplitude is linearly proportional to the force magnitude. The latter is proportional to the excitation light intensity and differential Raman polarizability for the mode being driven in the case of a Raman-like excitation, and to the pulse energy and the absorption coefficient for DECP. The coherent amplitude depends quadratically on inverse phonon frequency for both DECP and two-tensor models, whereas the dependence is linear for ISRS theory [10,13]. An exponential term in the DECP mechanism, hidden in the erfc function of Eq. (4), is explicitly independent of phonon frequency, while the similar term in both Raman models is controlled by the phonon frequency  $\Omega$  [13]. The latter property is the only sizable difference between the DECP and two-tensor models. However, since the complementary error function does depend implicitly on the phonon frequency  $\Omega$  through a lower bound of the definite integral, its contribution might be reduced to  $\exp(-\Omega^2 \tau_p^2/4)$  [14]. This feature makes the coherent amplitude dependence on pulse duration and phonon frequency identical for both DECP and two-tensor models. The arguments here are not rigorous, but hopefully, give the sense that the coherent amplitude relies on phonon frequency also in the displacive case. Nevertheless, in contrast to an impulsive force, in the displacive limit  $\Omega$  controls the displacement due to restoring force, which balances the driving force during the interaction time.

### III. EXPERIMENT

The crystals studied in our work belong to the class of layered materials. Because the layered crystals cleave easily between the layers, single crystals with the exposed basal ( $xy$ ) plane are readily obtained. Therefore, the optical measurements were carried out on  $\text{Bi}_2\text{Te}_3$ , Bi, and Sb single crystals cleaved perpendicular to the trigonal axis. No cleavage was necessary for Te single crystal as it possesses naturally exposed trigonal faces with optical quality surfaces. The crystals were glued with silver paste on the cold finger of an optical cryostat. The measurements on semimetals were carried out at  $T = 90$  K, which is lower than the Debye temperature of any of the crystals.  $\text{Bi}_2\text{Te}_3$  and Te crystals were studied at room temperature.

The pump-probe setup includes a mode-locked Ti:sapphire laser system with the pulse duration of 45 fs, a repetition rate of 80 MHz, and a center wavelength of 800 nm. Part of the laser beam was used as the pump pulse, while the remaining part served as the probe pulse. Small transient reflectivity changes of the probe beam were detected by using a photodiode and a lock-in amplifier (pump beam was modulated at 2 kHz with an optical chopper) [15]. The pump pulse can be tailored with a pulse shaper [16]. It involves a spatial Fourier transformation of the incident pulse to disperse the frequencies in space and modify the chosen frequency components selectively, while a final recombination of all the frequencies into a single, collimated beam results in the desired pulse duration. We employed the isotropic detection scheme in which the differential reflectance of the probe light,  $\Delta R/R_0 = (R - R_0)/R_0$  was defined as the relative change caused by the pump pulse with  $R_0$  being the reflectance at negative time delays. This isotropic detection allows coupling exclusively to the diagonal elements of the phonon Raman tensor. A linear motor stage was used to vary the delay time between the pump and probe pulses, and the polarizations of pump and probe beams were orthogonal to each other; meanwhile, both were perpendicular to the trigonal axis of the single crystal under study. Typically, the crystal was excited with 50 mW average pump power focused to a spot with a diameter of  $\approx 70 \mu\text{m}$  (the estimated pump fluence was around  $40 \mu\text{J}/\text{cm}^2$ ), while the probe power does not exceed 5 mW focused into a smaller spot.

Raman spectra were recorded on a micro-Raman spectrometer (Microdil-28) in a backscattering configuration. The spectra were excited with a visible laser light ( $\lambda = 632.8$  nm) at low power levels measured with the power meter at the sample position. The low power levels were essential to avoid local laser heating and damage. All the spectra were collected through a  $50\times$  objective and recorded with 1800 lines/mm grating and slit widths providing a spectral resolution better than  $1 \text{ cm}^{-1}$ . The spectra were recorded with the multichannel, nitrogen-cooled CCD detector positioned after the spectrograph.

### IV. RESULTS AND DISCUSSION

Having established how coherent amplitudes depend on experimentally controlled parameters, let us compare the theory predictions to what is observed in the time domain.

Thus, our strategy for testing the adequacy of the two-tensor model is to check the coherent amplitude dependence on phonon frequency, pulse width, and pulse power. First, consider the topological insulator  $\text{Bi}_2\text{Te}_3$  in which the phonon spectrum includes two fully symmetric modes [13,17,18]. Such set of phonons allows the comparison of coherent phonons of the same symmetry, both presumably driven by the same, displacive mechanism. Indeed, bismuth telluride crystallizes in rhombohedral  $D_{3d}^5$  structure and has six Raman-active phonons: a pair of fully symmetric  $A_{1g}$  and a pair of doubly degenerate  $E_g$  phonons whose frequencies follow in a descending order:  $A_{1g}^{(II)}$ ,  $E_g^{(II)}$ ,  $A_{1g}^{(I)}$ , and  $E_g^{(I)}$  [17]. In the high-symmetry modes, the atoms move along the trigonal axis. The difference between the two fully symmetric phonons is that the top two layers vibrate in phase in  $A_{1g}^{(I)}$  and out of phase in  $A_{1g}^{(II)}$ . Figure 1 shows the transient reflectance of  $\text{Bi}_2\text{Te}_3$  crystal at room temperature after the excitation with a 45 fs laser pulse. The reflectivity signal consists of a nonoscillatory background, the initial drop and a slower recovery, related to electron excitation and lattice heating via electron-lattice coupling, and oscillatory components appearing right after laser excitation. The maximum of the nonoscillatory response is shifted in time with respect to the zero delay determined by the pump-probe cross correlation. This shift is caused by the specifics of electronic structure [11]. Parameters of the ultrafast response were determined by fitting the time-domain data to a set of damped harmonic oscillators and a nonoscillating component

$$\frac{\Delta R}{R_0} = A_{el} \left[ \exp\left(-\frac{t}{\tau_{rise}}\right) - \exp\left(-\frac{t}{\tau_{rel}}\right) \right] + \sum_i A_i \exp\left(-\frac{t}{\tau_i}\right) \sin(2\pi \Omega_i t + \phi_i), \quad (11)$$

where  $A_{el}$  is the amplitude from photoexcited carriers;  $\tau_{rel}$  and  $\tau_{rise}$  are the relaxation and rising time, respectively;  $A_i$  is the coherent amplitude;  $\Omega_i$  is the frequency;  $\tau_i$  is the dephasing time; and  $\phi_i$  is the initial phase of the particular coherent phonon. Such decomposition allows comparison of the phonon  $A_i$  and electronic  $A_{el}$  parts needed to test the theory predictions. Having made the separation of the experimental signal into the sum of an electronic term and a phonon term, we then proceed to study each contribution.

The phonon (coherent)  $A_i$  and electronic (incoherent)  $A_{el}$  contributions are comparable to each other. The amplitude Fourier transform of a coherent component, performed after subtracting the nonoscillating transient and shown in Fig. 1(b), reveals slow and fast fully symmetric oscillations at 1.85 and 3.96 THz due to  $A_{1g}^{(I)}$  and  $A_{1g}^{(II)}$  phonons. Both fully symmetric phonons of  $\text{Bi}_2\text{Te}_3$  exhibit cosine dependence which physically implies that at the moment of excitation the atoms are maximally displaced from their equilibriums. According to the earlier studies [17–19], the cosinelike initial phase of the fully symmetric modes suggests the kinematic type of excitation.

The fully symmetric  $A_{1g}^{(I)}$  and  $A_{1g}^{(II)}$  Raman polarizabilities, obtained from the Raman spectrum shown in Fig. 1(c) and estimated via the integrated intensity, are related to each other as 3 to 4, which is also consistent with previous

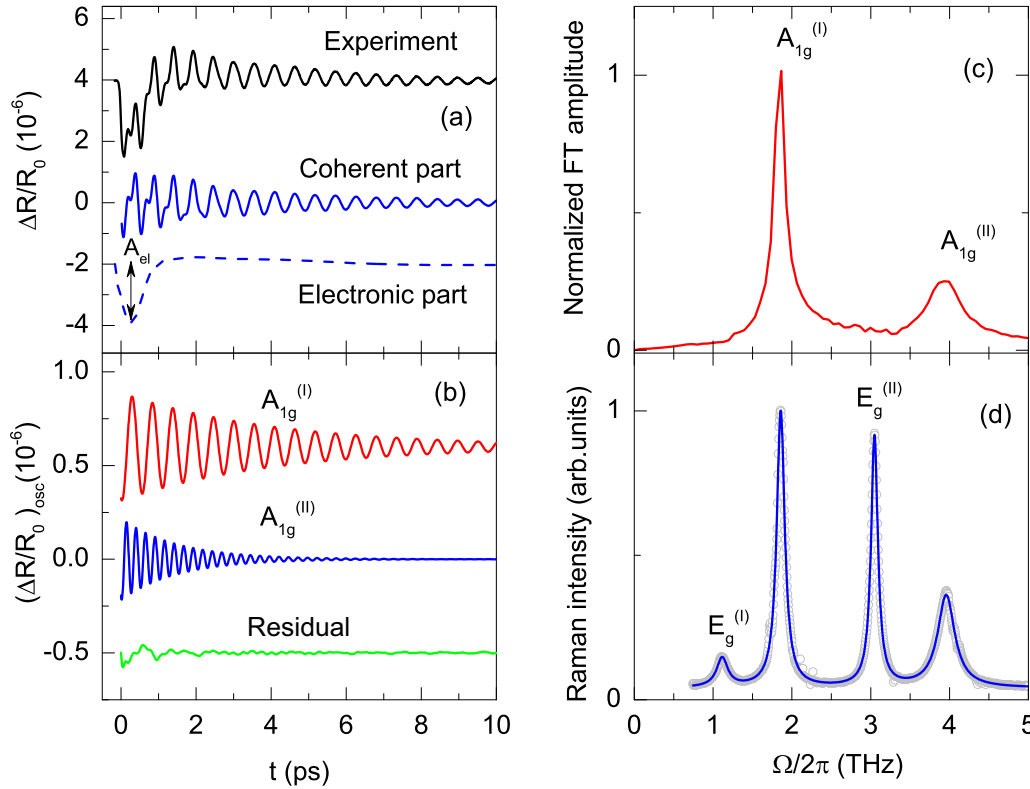


FIG. 1. (a) A typical differential change of the reflectance in  $\text{Bi}_2\text{Te}_3$  and its decomposition into coherent oscillations and electronic contribution. The data were taken at room temperature and detected with isotropic detection scheme. The curves are shifted vertically for clarity. (b) The decomposition of coherent oscillations into the symmetry components and the residual shifted vertically for clarity. (c) Normalized fast Fourier transform (FT) spectrum of coherent oscillations. (d) Raman unpolarized spectra excited with He-Ne laser in backscattering geometry. The open symbols are experimental points; the solid line is a cumulative fit to four Lorentzian profiles.

studies [17,19]. The coherent amplitude ratio obtained in this experiment  $Q_0(A_g^{II})/Q_0(A_g^{I}) \approx 2$  almost coincides with the ISRS prediction  $Q_0(A_g^{I})/Q_0(A_g^{II}) = \Omega_{A_g^{II}}/\Omega_{A_g^{I}} \approx 2.1$  provided we assume the instantaneous excitation with infinitely short pulses. On the other hand, as the efficiency to generate coherent phonons is higher for lower frequency mode, the amplitude ratio  $Q_0(A_g^{I})/Q_0(A_g^{II}) = \Omega_{A_g^{II}}^2/\Omega_{A_g^{I}}^2$  is expected to be 4.5 for the DECP model (here we assume that  $e$ -ph coupling is the same for both modes), and  $Q_0(A_g^{I})/Q_0(A_g^{II}) = (\Omega_{A_g^{II}}^2/\Omega_{A_g^{I}}^2)(\chi_{A_g^{I}}^R/\chi_{A_g^{II}}^R) \approx 3.4$  for the two-tensor model. Given the uncertainty (at the level of 50%) in values of the ratios, better agreement between theoretical estimates and experiment would not be expected. Note that increasing the pulse duration seems to result in an increase of the coherent amplitude ratio. Indeed, analyzing the literature data and comparing them to the ratios obtained in nondegenerate ultrafast pump-probe experiment [17–19], we see that with  $\tau_p = 70$  fs  $Q_0(A_g^{I})/Q_0(A_g^{II}) \approx 3.3$  [18], whereas with the pulse duration of 100 fs the ratio is larger than ten [19]. From the comparison, we infer the low-frequency and high-frequency modes grow at a different speed for decreasing pulse duration. Nevertheless, many other experimental conditions such as laser wavelength, pump intensity, spot size, temperature, etc., were different in [18,19], therefore, to confirm the coherent amplitude dependence on pulse duration in the topological insulator, the experiment should be carried out under identical

conditions. Such experiments will be described below for two semimetals and a semiconductor.

We now briefly address low-symmetry phonons in  $\text{Bi}_2\text{Te}_3$  that can only be driven by a Raman mechanism. For  $\lambda = 800$ nm excitation, the doubly degenerate phonons are absent in the isotropic detection scheme, but can be detected in the anisotropic detection [13,17]. In any case, their coherent amplitudes are one order of magnitude smaller than those of fully symmetric phonons. For a near-infrared excitation, the  $E_g^{(I)}$  and  $E_g^{(II)}$  amplitudes in the time domain are almost equal [19]. At the same time, their Raman  $E_g^{(II)}$  and  $E_g^{(I)}$  polarizabilities are related to each other as  $E_g^{(I)} : E_g^{(II)} \approx 7 : 1$ , signaling that the polarizability of high-frequency mode significantly exceeds that of low-frequency mode. The coherent amplitude ratio for these modes can be only attained by the two-tensor model for which  $Q_0(E_g^{I})/Q_0(E_g^{II}) = (\Omega_{E_g^{II}}^2/\Omega_{E_g^{I}}^2)(\chi_{E_g^{I}}^R/\chi_{E_g^{II}}^R) \approx 0.9$ . A significant difference between the fully symmetric and low-symmetry coherent amplitudes is naturally explained within the framework of the two-tensor model by including the driving force lifetime. Indeed, assuming that the dispersive force due to a Gaussian pump pulse exponentially decays with time

$$F(t) \propto \text{erfc}\left(\frac{\Gamma\tau_p}{2} - \frac{t}{\tau_p}\right) e^{[(\frac{\Gamma^2\tau_p^2}{4}) - \Gamma t]}, \quad (12)$$

we can see that when  $\Gamma$  exceeds the pulse duration  $\tau_p$ , the force is immensely suppressed [13]. As the  $E_g$  phonons in the

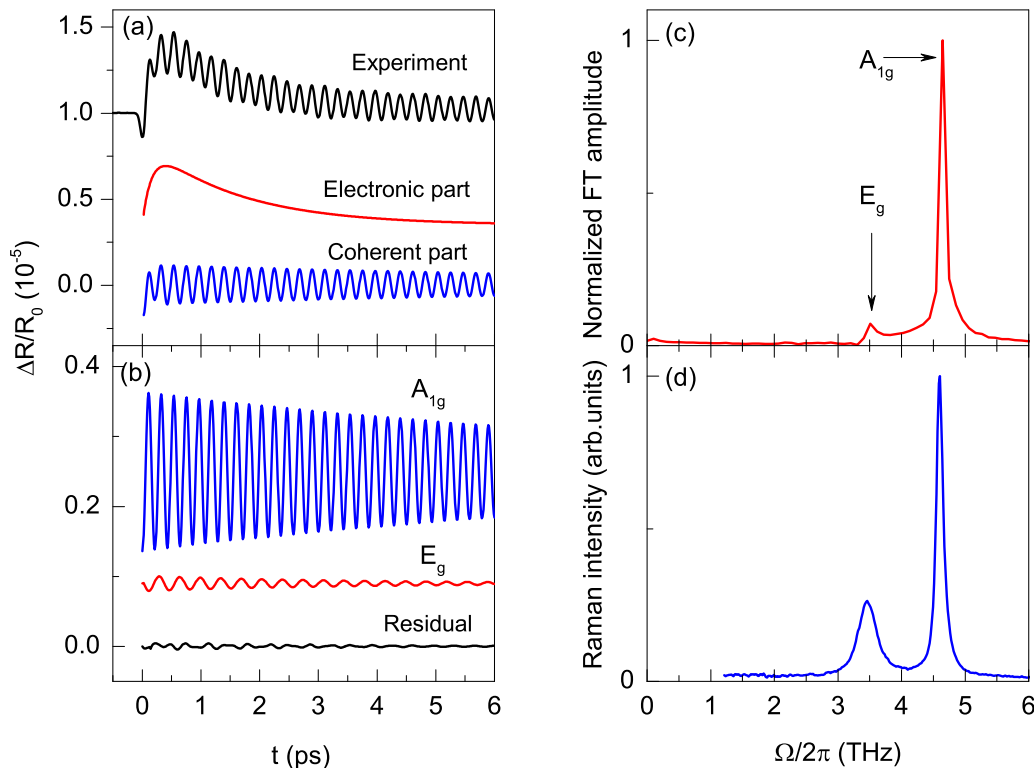


FIG. 2. (a) A typical differential change of the reflectance in Sb taken at 90 K with isotropic detection scheme and its decomposition into coherent oscillations and electronic contribution. The average pump power is  $-20$  mW; the pulse duration is  $-45$  fs. The curves are shifted vertically for clarity. (b) The decomposition of coherent oscillations into the symmetry components and the residual shifted vertically for clarity. (c) Normalized fast FT spectrum of coherent oscillations. (d) Raman unpolarized spectra excited with He-Ne laser at  $T = 90$  K in backscattering geometry with an electric field parallel to the bisectrix axis.

opaque crystals couple to low-symmetry components of the charge density, which usually decay on a time scale shorter than the oscillation period, their amplitudes are significantly smaller than those for fully symmetric phonons. For example, the anisotropic charge-density component in  $\text{Bi}_2\text{Te}_3$  decays within a time less than 10 fs [13,19], which is significantly shorter than the lifetime for isotropic charge density. Similarly, a much shorter lifetime (less than 10 fs) has been observed for  $E_g$  phonons in both semimetals, Sb and Bi [13,20], in which the isotropic charge-density component exists for the time around a few picoseconds. It has been suggested the  $E_g$  driving force decays so fast that the force fails to build up, rendering a weaker coherent phonon signal [13,20]. Note, however, that such short lifetime, encompassing only two to three optical cycles, appears to be incompatible with resonant excitation character. Nevertheless, the results of recent first-principle calculations of the polarization-dependent atomic forces [21] are in excellent agreement with those derived from measurements of the  $E_g$  amplitude and the anisotropic decay time of several femtoseconds [13,20].

To conclude, coherent lattice dynamics in  $\text{Bi}_2\text{Te}_3$  for both fully symmetric and doubly degenerate phonons is satisfactorily explained by the two-tensor model. Fully symmetric coherent lattice dynamics is also consistent with the DECP model, the predictions of which coincide with those of the two-tensor model.

Having considered multiple modes of the same symmetry, we then carried out degenerate femtosecond pump-probe

measurements in semimetals Sb and Bi and a semiconductor Te. This study substantiates our conjecture of a Raman-like generation of lattice coherence in the opaque crystals. We intentionally selected three exemplary materials whose coherent lattice dynamics laid a basis for the development of the DECP model to check the predictions of both DECP and two-tensor models. For this purpose, we will concentrate on the changes introduced by the variation of pump pulse duration at constant average pump power. We will then compare them to the changes when the pump duration is fixed and the average pump power is varied.

As already mentioned, the semimetals, bismuth and antimony, are the model objects for the study of coherent lattice dynamics in the opaque crystals [2,4,22–31]. Their coherent phonons [27,28] initiated the development of the DECP model [5] and, a little later, were used to justify the two-tensor model [7,8,20]. Both of the semimetals crystallize in the  $A7$  structure with two atoms in the primitive rhombohedral unit cell. Of their six phonons, the optic  $A_{1g}$  and  $E_g$  phonons are Raman active. The fully symmetric  $A_{1g}$  phonons of rhombohedral semimetals are formed by out-of-phase displacements of atoms along the trigonal axis, which modulate the internal (Peierls) shift. In a parent cubic lattice, these displacements coincide with those of longitudinal acoustic mode at the  $R$  corner of the Brillouin zone. The low-symmetry  $A7$  structure of these semimetals is primarily due to Peierls distortion, and the generation of fully symmetric coherent phonons can be considered as an inverse Peierls effect [5,29].

Figure 2(a) demonstrates the typical optical response of Sb to femtosecond excitation obtained in the isotropic detection scheme at  $T = 90$  K. Making fit to Eq. (9), we separate oscillating and nonoscillating parts and further decompose the coherent signal into two symmetry components as shown in Fig. 2(b). In Fig. 2(d), we present a Raman spectrum that shows two phonons of different symmetry, of which the fully symmetric one is dominant. From the time-domain data, we can see that the excited electrons, with a rise time of a few hundred femtoseconds, relax to the equilibrium state in a time of the order of a few picoseconds. On this electronic relaxation are superimposed oscillations generated by coherent optic phonons. From the ratio between the electron and coherent amplitudes, it follows that the electron and phonon contributions are comparable, although the former slightly dominates. Fourier analysis of coherent oscillations shown in Fig. 2(c) reveals that the main contribution comes from a fully symmetric  $A_{1g}$  phonon with the frequency of 4.63 THz. Note that its initial phase is close to  $-\pi/2$  as shown in Fig. 3(b), while that of lower symmetry phonon is almost zero, both consistent with the previous studies [4,26,31]. Such initial phases are qualitatively well accounted for by the two-tensor model (the  $A_{1g}$  phase is also consistent with DECP).

To further test the relationship between DECP and two-tensor models, we studied the dependence of ultrafast response on pump pulse width. To this end, the photoinduced transient reflectance was measured at various pump pulse durations (ranging from 45 fs up to 250 fs) for the same average pump power. To change the pump pulse duration, we used an ultrafast pulse shaper, while the probe pulse was always transform limited with the duration of 45 fs. Already from experimentally obtained transient reflectance, whose typical representatives are presented in Fig. 3(a), it is clear that the increase in pulse duration leads to the decrease in coherent oscillation amplitude. These three curves in Fig. 3(a) are drawn to give a feeling of the sensitivity of coherent amplitudes with respect to the pulse width. From the results obtained from the fit to Eq. (12) and shown in Fig. 3(c), follow that the coherent  $A_{1g}$  amplitude decays exponentially with increasing pump pulse duration. The decay is exponential  $e^{-t/\tau}$  with the characteristic time  $\tau$  roughly equal to a quarter of phonon period ( $T = 226$  fs,  $\tau = 60$  fs). On the other hand, the electron contribution to the fully symmetric signal remains virtually unchanged for all varying pulse durations [see Fig. 3(c)]. Indeed, within the experimental errors, we did not detect a change in the position and magnitude of the electronic part  $A_{el}$ . Thus, contrary to the common belief that coherent amplitude is proportional to photoexcited carrier density, our results highlight situations in which they are uncorrelated. Interestingly, the lack of correlation between the fully symmetric electronic and lattice contributions can be also seen in the data reported in a temperature-dependent pump-probe study on Sb [30], but the authors did not discuss the origin of the observed effect. These observations might have refuted the DECP model in which the driving force for isotropic coherent lattice dynamics proportional to carrier density is due to a non-Raman process. Yet the carrier density in DECP is proportional to the pulse energy that remains almost constant in these experiments. What remains unclear is the lack of any correlation between

the phonon and electron contributions which according to Eq. (3) should be equal. However, in fact Eq. (3) describes only the lattice part [its counterpart is Eq. (5) in Ref. [5]]. The full original Eq. (21) in [5] is given by the sum of two terms

$$\frac{\Delta R}{R_0} = A \int_0^\infty g(t-\tau) d\tau + B \int_0^\infty g(t-\tau) \left\{ e^{-\Gamma\tau} - e^{-\gamma\tau} \left[ \cos(\tilde{\Omega}\tau) - \frac{\Gamma-\gamma}{\tilde{\Omega}} \sin(\tilde{\Omega}\tau) \right] \right\} d\tau, \quad (13)$$

where  $\tilde{\Omega} = \sqrt{\Omega^2 - \gamma^2}$  is the renormalized phonon frequency and  $g(t)$  is the laser pulse autocorrelation function. Relating  $A_{el}$  and  $A_i$  in Eq. (11) to the first and second terms of Eq. (13), respectively, one can see that the first term is the source driving the second. It is independent of pulse duration provided the pulse energy is conserved. The second term is the sum of the dc offset and oscillating parts in which the offset is independent of, whereas the oscillating part is dependent on pulse duration (because the longer pulses suppress the oscillations). Intuitively, the electron contribution formed by a transient absorption remains constant for the pulse durations satisfying the inequality  $1/\Gamma > \tau_p > 0$ , while the coherent amplitude should depend on the shape of the pump pulse. The coherent amplitude contribution attains its maximum value when the pulse envelope can be considered as a  $\delta$  function, that is, in the limit  $\Omega\tau_p \rightarrow 0$ . By increasing the pulse duration toward the adiabatic limit  $\Omega\tau_p \rightarrow \infty$ , the coherent amplitude is expected to approach monotonically zero. One of the ways to understand such a behavior is to conjecture the atoms move on the excited potential surface during the pulse duration. Therefore, for longer interaction times controlled by the pulse width, the atoms can move closer to the newly created potential minimum resulting in smaller coherent amplitude for the same shift of the potential. This idea has been advanced in the ultrafast study of  $A_{1g}$  coherent phonons in  $\text{TiO}_2$  [32] to explain a shift in the initial phase with respect to the instantaneous displacive excitation,  $\Omega\tau_p \rightarrow 0$ . Unfortunately, the experimental accuracy of 10%–15% in the determination of zero delay time does not allow us to detect the initial phase shift as well as a change of the rise time for longer pump pulses.

To check further the theory predictions, the coherent amplitude dependence on pump intensity, in which we varied the average pump power keeping the pulse duration intact, was also measured. As shown in Fig. 3(d), both the electron and lattice contributions grow linearly without any threshold for increasing average power. This threshold absence is evidenced by a linear approximation extrapolated to the zero pump power and shown by a dashed line in Fig. 3(d). Such behavior can be explained by both theories. In the case of a Raman-like model, the threshold absence happens because the seed photons, produced in the continuous-wave stimulated Raman by a spontaneous process, for impulsive Raman excitation are originally present in the pump pulse. On the other hand, the linear increase of coherent amplitude with higher excitation might be a direct consequence of the DECP mechanism that launches the phonons. Indeed, impulsive absorption (both single- and two-photon), on which the DECP model resides, has only an *energy* threshold, but it is also linear with the

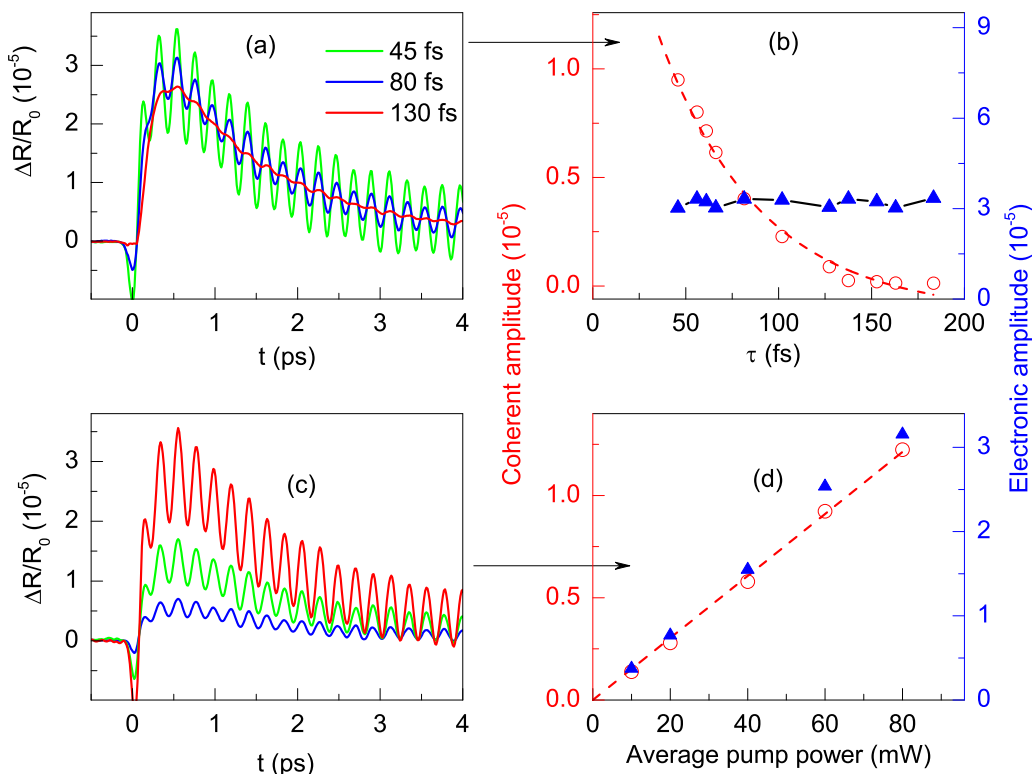


FIG. 3. (a) Typical differential change of the reflectance in Sb taken in a degenerate pump-probe experiment at 90 K with isotropic detection scheme for different pump pulse durations. (b) Coherent amplitude (open symbols) and electronic contribution (closed triangles) as a function of pump pulse duration. The dashed line is an exponential fit to coherent amplitude data. (c) Typical differential change of the reflectance in Sb taken with different average pump pulse powers (from the bottom to the top: 20, 40, and 80 mW, respectively). (d) Pump-power dependence for coherent (open symbols) and incoherent (closed triangles) parts. The dashed line is a linear fit to coherent amplitude data.

excitation intensity. Interestingly, in contrast to the pulse duration dependence, for the pump-power dependence we observed a decrease in the electronic rise time for larger pump powers. This feature is consistent with the previous pump-probe experiments on Sb in which the position and magnitude of electronic parts depend on both pump power and temperature [11]. In particular, the peak position  $A_{el}$  at low temperature shifts toward smaller delays with increasing pump intensity [11].

As a consistency check, the ultrafast measurements were repeated for bismuth. In Bi, the similar behavior for both lattice and electron contributions was observed. The Bi results obtained at the same temperature are summarily presented in Fig. 4. From Figs. 4(a) and 4(c) we can see that fully symmetric  $A_{1g}$  phonons with the frequency of 3.01 THz demonstrate the increase in coherent amplitude and independence of electronic contribution for shorter pulse durations. The coherent amplitude in Bi obeys the similar as in Sb dependence on pulse duration decaying exponentially with the characteristic time equal to a quarter of  $A_{1g}$  phonon period ( $T = 332$  fs,  $\tau = 80$  fs). Also for fixed pulse duration, both coherent and electronic contributions grow linearly with average pump power without any threshold [see Fig. 4(d)]. Finally, we should note that the results obtained in the pump power and pulse duration dependence for bismuth also manifest independence of  $A_{1g}$  phonon frequency, decay rate, and initial phase on the varied variable. This independence signals that we are in a linear regime [15].

To finish, a similar set of pump-probe experiments was carried out for  $\alpha$ -Te in which we observed the same behavior as in the semimetals for both the lattice and electron contributions. Tellurium crystallizes with three atoms per unit cell in which twofold-coordinated Te atoms form infinite helical chains parallel to the  $c$  axis of the trigonal  $D_3^4$  structure [16,33]. Each helix is surrounded by six equidistant helices and each atom has four second-nearest neighbors in these adjacent helices. The single atomic position free parameter is equal to the ratio of the radius of each helix to the interhelical distance. Since the parameter value is not determined by symmetry, the equilibrium value is, therefore, sensitive to the precise details of electronic structure. The  $\alpha$ -Te crystal structure may be viewed as a Peierls distortion [33] of the  $\gamma$ -Te rhombohedral structure ( $D_{3d}^5$  with one atom per unit cell), the same way as the semimetals rhombohedral structures can be considered as a Peierls distortion of the cubic structure. This feature allows for a coherent excitation of the  $A_1$  phonons via the DECP mechanism since any change in the electronic state occupation alters the free parameter value [5,33]. Among six optic phonons of  $\alpha$ -Te, the  $A_1$  phonon with the frequency of  $\approx 3.6$  THz corresponds to the symmetric intrachain dilation and compression normal to the chain axis. This Peierls-like  $A_1$  mode is the dominant contribution in the ultrafast pump-probe experiment, the results of which are summarily shown in Fig. 5. The  $A_1$  phonons display a cosine dependence. As is evident from Fig. 5(b), they exhibit the exponential increase in coherent amplitude, with the temporal constant equal to

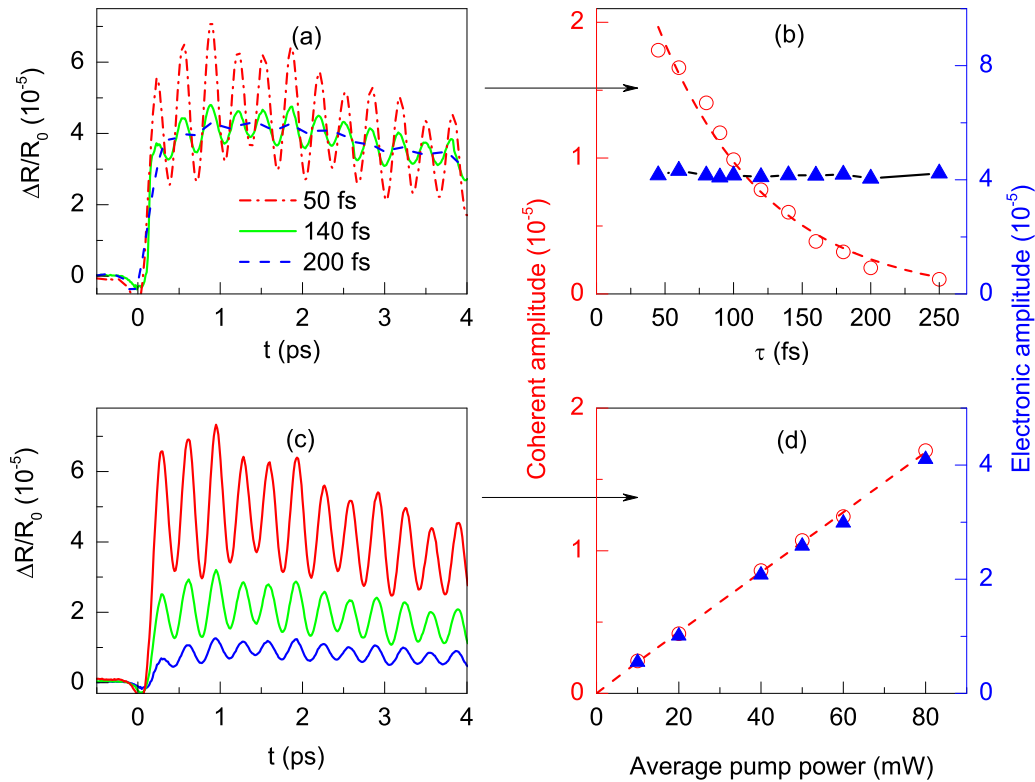


FIG. 4. (a) Typical differential change of the reflectance in Bi taken in a degenerate pump-probe experiment at 90 K with isotropic detection scheme for different pump pulse durations. (b) Coherent amplitude (open symbols) and electronic contribution (closed triangles) as a function of pump pulse duration. The dashed line is an exponential fit to coherent amplitude data. (c) Typical differential change of the reflectance  $n$  in Bi taken with different pump pulse powers (from the bottom to the top: 20, 40, and 80 mW, respectively). (d) Pump-power dependence for coherent (open symbols) and incoherent (closed triangles) parts. The dashed line is a linear fit to coherent amplitude data.

a quarter of inverse phonon period, and independence of electronic contribution for shorter pulse duration. For fixed pulse duration, both the coherent and electronic contributions grow linearly with average pump power without any threshold as shown in Fig. 5(c).

Finally, we split the 50 fs transform-limited pump pulse into two identical Gaussian pulses with the same energy to carry out coherent control experiment. Figure 5(a) shows the transient reflectance of  $\alpha$ -Te excited with such two-pulse sequence with the interpulse separation  $\alpha$  of 140 and 280 fs together with that excited by the single pump pulse. One can see that if the total electronic contribution is always the sum of the signals resulting from each pump pulse independently, the oscillatory component exhibits interferences resulting in a cancellation of the coherent amplitude for  $\alpha = 140$  fs as compared to single-pulse excitation. Thus, the data show that the particular double-pulse combination leads to cancellation or enhancement of the coherent phonons, whereas the electronic contribution remains essentially unchanged. This observation suggests that splitting the excitation energy (or the number of photons) between multiple pulses can provide selectivity, but not increase in the resulting coherent amplitude, suggesting that the lattice excitation is proportional to the total energy (or intensity) of the pump pulse. Unpretentiously, assuming a kinematic excitation, the coherent control process can be thought of as follows: The first pump pulse establishes a new potential surface on which the atoms move and the lattice, initially displaced from the

newly established equilibrium, achieves this configuration in approximately one-quarter of a phonon period, but the atoms have momentum at that point. When the atoms reach the classical turning point of their motion, a second pump pulse can excite the exact density of carriers to shift the equilibrium position to the current position of the atoms, thus removing the restoring force and stopping the oscillatory motion. Because ultrafast pulse can only shift the equilibrium position in one direction, the oscillations can only be stopped for time delays equal to an odd number of phonon semiperiods between pump pulses. For time delays equal to an even number of semiperiods the oscillations are enhanced. In the linear regime under weak excitation, this criterion has been verified experimentally in Bi [4,34,35].

It should be emphasized that all the results on semimetals and a semiconductor were obtained in a low fluence regime. The various effects in narrow-band materials like nonlinearity, anharmonicity, damping, etc., can become comparable in importance to the effects present in the linear regime and result in frequency chirp, nonlinear amplitudes, and modified decay of coherent phonons [4,13,16,36–38]. It may be interesting to sort out the influence of these effects in a future study. Furthermore, as suggested previously [38], to reduce DECP to the resonance Raman scattering is only possible by merging the hot luminescence and resonant Raman scattering into a single mechanism. However, if in the Raman case the phonon creation can occur both before and after absorption of a photon, in the

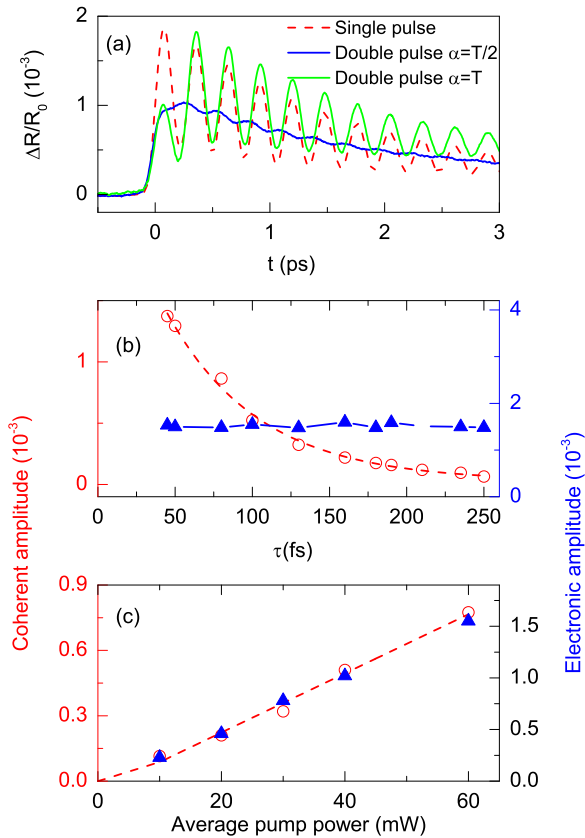


FIG. 5. (a) Coherent control in Te. The signal of a single-pulse excitation is compared with a two-pulse sequence of the same total energy. The interpulse separations  $\alpha$  are 140 and 280 fs. (b) Coherent amplitude (open symbols) and electronic contribution (closed triangles) as a function of pump pulse duration for  $A_1$  phonons in Te. The dashed line is an exponential fit to coherent amplitude data. (c) Pump-power dependence for coherent (open symbols) and incoherent (closed triangles) fully symmetric parts. The dashed line is a linear fit to coherent amplitude data.

hot luminescence, the phonon creation takes place only after the photon absorption. This reduces the number of possible ways of ordering the Feynman diagram vertices, leading to significant differences in the probability of the elementary scattering act. Raman scattering is a two-photon direct process, while hot luminescence, and its analog in the time domain—DECP, is a two-step process that essentially depends on the photoexcited carrier relaxation [38]. The main difference between Raman scattering and hot luminescence is that the former is determined by the transverse relaxation, while the latter is controlled by the longitudinal relaxation generating the lattice coherence due to a rapid nonradiative process [38,39]. Nevertheless, the treatment of hot luminescence as a Raman process in which the phonon creation occurs only after the photon absorption allows the two-tensor model to be a unified model for the description of coherent phonon generation in both opaque and transparent regimes. The usage of a complex Raman tensor in the two-tensor model can be put side by side with the Raman measurements carried out with polarization vectors of the incident and scattered light not parallel to the principal axes of the second rank tensor. In contrast to

measuring the phonon Raman intensity with the polarization vectors along the crystal principal axes, which corresponds to the determination of the absolute tensor component value only with the phase information escaped from the measuring process, when the polarizations are not parallel to the crystal axes, the relative phase difference between Raman tensor elements affects the scattering strength [40]. Similarly, in the case of Fano interference between the phonon and the electronic continuum, the sign of phonon tensor component, which can be related to its phase, regulates the position of antiresonance in the spontaneous Raman spectrum [41] and controls the initial phase of coherent phonons in the time domain [42,43].

In passing, let us also comment on the coherent amplitude dependence on pulse duration. Recall that it has long been suspected that there might be optimal pulse duration for coherent phonon generation [14,44–47]. The appearance of such optimal duration is easily explained by a toy model. Assume the pendulum has a period of  $T$  and initially is in its equilibrium position. The key is that the driving force can excite it most effectively in the first quarter of its period, i.e.,  $T/4$ . If the force duration is longer or shorter than  $T/4$ , this pendulum will not achieve the maximal amplitude. Consequently, the theoretical ratio of the pendulum period  $T$  to the driving force duration  $\tau$  is expected to be four. More sophisticated theoretical models [14,44–47] suggest larger optimal pulse duration. For example, in Ref. [15] it was found that the optimum value of  $\tau_p$  was about  $0.42T$ , whereas in Ref. [45]  $\tau_p \leq 0.4T$ . However, the theoretical results seem to be inconsistent with the existing experiments on opaque crystals [4,31,48,49] as well as with our study that rules out the existence of a maximum at least for the pulse durations larger than  $0.15\text{--}0.2 T$ . Here it is appropriate to mention that according to theoretical model [14], the optimal pulse duration exists only for a Raman-like excitation and is absent for DECP. Nevertheless, the recent experimental study [31] fails to observe the optimal pump pulse duration for coherent phonons excited either via DECP, or ISRS (in both cases, the coherent amplitude decreases monotonically with respect to pulse duration, without any maximum). A way to quantitatively characterize how strongly the phonons are excited in different theories [14,45–47], via an estimate of the potential or kinetic energy, does not seem to be important, as in a low fluence excitation regime used in our study, the potential surface anharmonicity can be neglected [45]. On the other hand, the universal dependence  $\tau = T/4$ , observed in all opaque crystals for the varying pulse widths, can be an indication that the atoms start their movement with zero velocity and the restoring force is controlled by the potential steepness proportional to the phonon frequency—the steeper the potential, the faster the amplitude decays.

Based on the experimental results obtained, it can be claimed that the two-tensor model correctly describes the generation of lattice coherence for any Raman-active phonon in opaque materials. The experimental results allow conjecturing that this lattice coherence is due to the transfer of coherence between light and lattice. DECP, on the other hand, is able to explain the generation of fully symmetric coherent phonons for which the DECP predictions coincide with experiment and predictions of the two-tensor model.

Thus, the two-tensor model does provide a unifying approach for describing the coherent motion of atoms of both impulsive and displacive character. The comparison shows that DECP and two-tensor theories are very similar, differing mainly in the coherent amplitude dependence on pump pulse structure, which seems to be a single significant distinction. While DECP relies exclusively on the temporal pulse envelope, the two-tensor model, in addition, depends explicitly on the pulse spectrum. Including the hot luminescence, which is controlled by the pulse envelope and generates the lattice coherence due to rapid nonradiative processes, into a Raman framework makes the two-tensor model identical to DECP. We also would like to stress that in this work we concentrate on the generation mechanism for fully symmetric phonons in the opaque materials and do not consider the detection mechanism that is always a Raman-like process [1,5,50–52].

## V. CONCLUSION

To summarize, the ultrafast pump-probe experiments in  $\text{Bi}_2\text{Te}_3$ , Sb, Bi, and Te all show similar features that support the validity of the two-tensor model. The latter three materials, where DECP was previously identified as the generating mechanism, were intentionally chosen to compare their coherent lattice dynamics with the two-tensor model predictions. All fully symmetric coherent phonons exhibit a cosine

dependence indicative of displacive (kinematic) excitation which is consistent with both DECP and two-tensor models. Their coherent amplitudes grow linearly with increasing pump intensity provided the pulse duration remains unchanged, the feature also predicted by both models. Varying the pump pulse duration, we observed the monotonic decrease of coherent amplitude for longer pulses in Sb, Bi, and Te, whereas the electronic contribution was barely changed. This lack of the correlation between the carriers and the coherent amplitude was further supported by coherent control experiments on Te. To explain why the electron and phonon contributions, if the former drives the latter, react differently to pulse duration, we conjecture that this feature can be explained by the movement of atoms during the interaction time. The electronic contribution does determine the maximal coherent phonon amplitude attained with infinitely short pulses at the instantaneous displacive excitation,  $\Omega\tau_p \rightarrow 0$ . However, the correlation between the electron and phonon contributions disappears for longer pulses because the former is independent of, while the latter is dependent on pump pulse duration.

## ACKNOWLEDGMENTS

The work was supported in part by the Russian Foundation for Basic Research under Grants No. 14-02-00105-a and No. 14-42-03576-p. Stimulating discussions with A. A. Melnikov are also acknowledged.

- 
- [1] L. Dhar, J. A. Rogers, and K. A. Nelson, Time-resolved vibrational spectroscopy in the impulsive limit, *Chem. Rev.* **94**, 157 (1994).
- [2] R. Merlin, Generating coherent THz phonons with light pulses, *Solid State Commun.* **102**, 207 (1997).
- [3] T. Dekorsy, G. C. Cho, and H. Kurz, Coherent phonons in condensed media, in *Light Scattering in Solids VIII*, edited by M. Cardona and G. Guentherodt (Springer, Berlin, 2000), pp. 169–209.
- [4] K. Ishioka and O. V. Misochko, Coherent lattice oscillations in solids and their optical control, in *Progress in Ultrafast Intense Laser Science V*, edited by K. Yamanouchi, A. Giullietti, and K. Ledingham, Springer Series in Chemical Physics (Springer, Berlin, 2010), pp. 23–64.
- [5] H. J. Zeiger, J. Vidal, T. K. Cheng, E. P. Ippen, G. Dresselhaus, and M. S. Dresselhaus, Theory for displacive excitation of coherent phonons, *Phys. Rev. B* **45**, 768 (1992).
- [6] N. Bloembergen, From nanosecond to femtosecond science, *Rev. Mod. Phys.* **71**, S283 (1999).
- [7] G. A. Garrett, T. F. Albrecht, J. F. Whitaker, and R. Merlin, Coherent THz Phonons Driven by Light Pulses and the Sb Problem: What is the Mechanism?, *Phys. Rev. Lett.* **77**, 3661 (1996).
- [8] T. E. Stevens, J. Kuhl, and R. Merlin, Coherent phonon generation and the two stimulated Raman tensors, *Phys. Rev. B* **65**, 144304 (2002).
- [9] R. A. Bartels, S. Backus, M. M. Murnane, and H. C. Kapteyn, Impulsive stimulated Raman scattering of molecular vibrations using nonlinear pulse shaping, *Chem. Phys. Lett.* **374**, 326 (2003).
- [10] A. Nazarkin and G. Korn, Raman self-conversion of femtosecond laser pulses and generation of single-cycle radiation, *Phys. Rev. A* **58**, R61 (1998).
- [11] M. V. Lebedev and O. V. Misochko, Generation of coherent phonons in opaque crystals: A radio engineering analogy, *Phys. Solid State* **51**, 1843 (2009).
- [12] D. M. Riffe and A. J. Sabbah, Coherent excitation of the optic phonon in Si: Transiently stimulated Raman scattering with a finite-lifetime electronic excitation, *Phys. Rev. B* **76**, 085207 (2007).
- [13] J. Li, Ultrafast and incoherent Raman studies of optical phonons of different symmetries in Sb, Bi,  $\text{Bi}_2\text{Te}_3$  and  $\text{Bi}_2\text{Se}_3$ , Ph.D. dissertation, University of Michigan, 2012.
- [14] K. G. Nakamura, Y. Shikano, and Y. Kayanuma, Influence of pulse width and detuning on coherent phonon generation, *Phys. Rev. B* **92**, 144304 (2015).
- [15] O. V. Misochko and M. V. Lebedev, Investigation of the dependence of the coherent dynamics of a bismuth lattice on the crystal excitation level, *J. Exp. Theor. Phys.* **109**, 805 (2009).
- [16] O. V. Misochko, M. V. Lebedev, H. Shaeffer, and T. Dekorsy, Coherent  $A_1$  phonons in Te studied with tailored femtosecond pulses, *J. Phys.: Condens. Matter.* **19**, 406220 (2007).
- [17] O. V. Misochko, J. Flock, and T. Dekorsy, Polarization dependence of coherent phonon generation and detection in the three-dimensional topological insulator  $\text{Bi}_2\text{Te}_3$ , *Phys. Rev. B* **91**, 174303 (2015).

- [18] A. Q. Wu, X. Xu, and R. Venkatasubramanian, Ultrafast dynamics of photoexcited coherent phonon in  $\text{Bi}_2\text{Te}_3$  thin films, *Appl. Phys. Lett.* **92**, 011108 (2008).
- [19] O. V. Misochko, A. A. Mel'nikov, S. V. Chekalin, and A. Yu. Bykov, Features of coherent phonons of the strong topological insulator  $\text{Bi}_2\text{Te}_3$ , *JETP Lett.* **102**, 235 (2015).
- [20] J. J. Li, J. Chen, D. A. Reis, S. Fahy, and R. Merlin, Optical Probing of Ultrafast Electronic Decay in Bi and Sb with Slow Phonons, *Phys. Rev. Lett.* **110**, 047401 (2013).
- [21] É. D. Murray and S. Fahy, First-Principles Calculation of Femtosecond Symmetry-Breaking Atomic Forces in Photoexcited Bismuth, *Phys. Rev. Lett.* **114**, 055502 (2015).
- [22] Muneaki Hase, K. Mizoguchi, H. Harima, S. Nakashima, and K. Sakai, Dynamics of coherent phonons in bismuth generated by ultrashort laser pulses, *Phys. Rev. B* **58**, 5448 (1998).
- [23] O. V. Misochko, K. Kisoda, K. Sakai, and S. Nakashima, Peculiar noise properties of phonons generated by femtosecond laser pulses in antimony, *Appl. Phys. Lett.* **76**, 961 (2000).
- [24] D. Boschetto, E. G. Gamaly, A. V. Rode, B. Luther-Davies, D. Glijer, T. Garl, O. Albert, A. Rousse, and J. Etchepare, Small Atomic Displacements Recorded in Bismuth by the Optical Reflectivity of Femtosecond Laser-Pulse Excitations, *Phys. Rev. Lett.* **100**, 027404 (2008).
- [25] K. Ishioka, M. Kitajima, and O. V. Misochko, Coherent  $A_{1g}$  and  $E_g$  phonons of antimony, *J. Appl. Phys.* **103**, 123505 (2008).
- [26] O. V. Misochko, K. Ishioka, Muneaki Hase, and M. Kitajima, Fully symmetric and doubly degenerate coherent phonons in semimetals at low temperature and high excitation: Similarities and differences, *J. Phys.: Condens. Matter* **18**, 10571 (2006).
- [27] T. H. Cheng, S. D. Brorson, A. S. Kazeroonian, J. S. Moodera, G. Dresselhaus, M. S. Dresselhaus, and E. P. Ippen, Impulsive excitation of coherent phonons observed in reflection in bismuth and antimony, *Appl. Phys. Lett.* **57**, 1004 (1990).
- [28] T. K. Cheng, J. Vidal, H. J. Zeiger, G. Dresselhaus, M. S. Dresselhaus, and E. P. Ippen, Mechanism for displacive excitation of coherent phonons in Sb, Bi, Te, and  $\text{Ti}_2\text{O}_3$ , *Appl. Phys. Lett.* **59**, 1923 (1991).
- [29] D. Fausti, O. V. Misochko, and P. H. M. van Loosdrecht, Ultrafast photoinduced structure phase transition in antimony single crystals, *Phys. Rev. B* **80**, 161207(R) (2009).
- [30] M. Hase, K. Ushida, and M. Kitajima, Anharmonic decay of coherent optical phonons in antimony, *J. Phys. Soc. Jpn.* **84**, 024708 (2015).
- [31] O. V. Misochko, Pump pulse duration dependence of coherent phonon amplitudes in antimony, *J. Exp. Theor. Phys.* **123**, 292 (2016).
- [32] E. M. Bothschafter, A. Paarmann, E. S. Zijlstra, N. Karpowicz, M. E. Garcia, R. Kienberger, and R. Ernstorfer, Ultrafast Evolution of the Excited-State Potential Energy Surface of  $\text{TiO}_2$  Single Crystals Induced by Carrier Cooling, *Phys. Rev. Lett.* **110**, 067402 (2013).
- [33] P. Tangney and S. Fahy, Density-functional theory approach to ultrafast laser excitation of semiconductors: Application to the  $A_1$  phonon in tellurium, *Phys. Rev. B* **65**, 054302 (2002).
- [34] M. Hase, K. Mizoguchi, H. Harima, S. Nakashima, M. Tani, K. Sakai, and M. Hangyo, Optical control of coherent optical phonons in bismuth films, *Appl. Phys. Lett.* **69**, 2474 (1996).
- [35] O. V. Misochko and M. V. Lebedev, Optical control of the coherent dynamics of a bismuth lattice at liquid-helium temperature at low and high excitation levels, *JETP Lett.* **90**, 284 (2009).
- [36] M. Hase, M. Kitajima, S. Nakashima, and K. Mizoguchi, Dynamics of Coherent Anharmonic Phonons in Bismuth Using High Density Photoexcitation, *Phys. Rev. Lett.* **88**, 067401 (2002).
- [37] J. P. Callan, A. M.-T. Kim, L. Huang, and E. Mazur, Ultrafast electron and lattice dynamics in semiconductors at high excited carrier densities, *Chem. Phys.* **251**, 167 (1998).
- [38] A. A. Melnikov, O. V. Misochko, and S. V. Chekalin, Generation of coherent phonons in bismuth by ultrashort laser pulses in the visible and NIR: Displacive versus impulsive excitation mechanism, *Phys. Lett. A* **375**, 2017 (2011).
- [39] Y. R. Shen, Distinction between resonance Raman scattering and hot luminescence, *Phys. Rev. B* **9**, 622 (1974).
- [40] T. Strach, J. Brunen, B. Lederle, J. Zegenhagen, and M. Cardona, *Phys. Rev. B* **57**, 1292 (1998).
- [41] M. Cardona, in *Light Scattering in Solids II*, edited by M. Cardona, and G. Guentherodt (Springer, Berlin, 1982).
- [42] D. M. Riffe, Classical Fano oscillator, *Phys. Rev. B* **84**, 064308 (2011).
- [43] O. V. Misochko and M. V. Lebedev, Fano interference at the excitation of coherent phonons: Relation between the asymmetry parameter and the initial phase of coherent oscillations, *J. Exp. Theor. Phys.* **120**, 651 (2015).
- [44] T. J. Smith and J. A. Cina, Toward preresonant impulsive Raman preparation of large amplitude vibrational motion, *J. Chem. Phys.* **104**, 1272 (1996).
- [45] G. P. Zhang and T. F. George, Controlling Vibrational Excitations in  $\text{C}_{60}$  by Laser Pulse Durations, *Phys. Rev. Lett.* **93**, 147401 (2004).
- [46] X. Zhou, Z. Lin, C. Jiang, M. Gao, and R. E. Allen, Maximum relative excitation of a specific vibrational mode via optimum laser-pulse duration, *Phys. Rev. B* **82**, 075433 (2010).
- [47] T. Shimada, C. Frischkorn, M. Wolf, and T. Kampfrath, Maximizing the amplitude of coherent phonons with shaped laser pulses, *J. Appl. Phys.* **112**, 113103 (2012).
- [48] I. H. Lee, K. J. Yee, K. G. Lee, E. Oh, D. S. Kim, and Y. S. Lim, Coherent optical phonon mode oscillations in wurtzite  $\text{ZnO}$  excited by femtosecond pulses, *J. Appl. Phys.* **93**, 4939 (2003).
- [49] A. R. T. Nugraha, E. H. Hasdeo, G. D. Sanders, C. J. Stanton, and R. Saito, Origin of coherent  $G$ -band phonon spectra in single-wall carbon nanotubes, *Phys. Rev. B* **91**, 045406 (2015).
- [50] O. V. Misochko, Muneaki Hase, and M. Kitajima, Spectrally filtered time domain study of coherent phonons in semimetals, *J. Phys.: Condens. Matter* **16**, 1879 (2004).
- [51] R. Morishita, G. Oohata, and K. Mizoguchi, Anomalous detection-energy dependence of coherent phonon in bismuth thin films, *Phys. Status Solidi C* **8**, 169 (2011).
- [52] K. Mizoguchi, R. Morishita, and G. Oohata, Generation of Coherent Phonons in a  $\text{CdTe}$  Single Crystal Using an Ultrafast Two-Phonon Laser-Excitation Process, *Phys. Rev. Lett.* **110**, 077402 (2013).